Soft Matter

PAPER

View Article Online
View Journal | View Issue

Mechanical characterization of cross-linked serum albumin microcapsules†

Cite this: *Soft Matter*, 2014, **10**, 4561

Clément de Loubens,[a] Julien Deschamps,*[a] Marc Georgelin,[a] Anne Charrier,[b] Florence Edwards-Levy[c] and Marc Leonetti*[a]

Received 13th February 2014
Accepted 3rd April 2014

DOI: 10.1039/c4sm00349g

www.rsc.org/softmatter

Controlling the deformation of microcapsules and capsules is essential in numerous biomedical applications. The mechanical properties of the membrane of microcapsules made of cross-linked human serum albumin (HSA) are revealed by two complementary experiments in the linear elastic regime. The first provides the surfacic shear elastic modulus G_s by the study of small deformations of a single capsule trapped in an elongational flow: G_s varies from 0.002 to 5 N m^{-1}. The second gives the volumic Young's modulus E of the membrane by shallow and local indentations of the membrane with an AFM probe: E varies from 20 kPa to 1 MPa. The surfacic and volumic elastic moduli increase with the size of the capsule up to three orders of magnitude and with the protein concentration of the membrane. The membrane thickness is evaluated from these two membrane mechanical characteristics and increases with the size and the initial HSA concentration from 2 to 20 μm.

1 Introduction

Microencapsulation refers to diverse techniques to enclose active materials within a shell with the aim of protecting them from the outside and to control their spatiotemporal release. This process offers answers to many biotechnological challenges[1–3] such as cancer therapy[4] and cardiovascular treatments.[5] Various containers result from encapsulation of a droplet coated with a solid, such as polymeric capsules, or liquid membranes such as vesicles. The membrane may exhibit various mechanical properties that are essential for controlling the delivery of the active materials.[6–8] These characteristics are quite limited for fluid vesicles made of lipids:[9] the thickness is fixed by the lipid bilayer and their deformation is governed by bending rigidity and membrane incompressibility.[10] While the membrane viscosity is negligible for vesicles, polymersomes are also characterized by shear resistance.[11] The variety of geometrical and mechanical properties is widely increased for capsules made of polymers with weak or strong cross-linking. The membrane is supposed to exhibit a viscoelastic behavior and a bending resistance. These characteristics depend on both the chemical composition of the membrane and the preparation process. Understanding the role of the process on the mechanical properties of the membrane is thus of prime importance.

Various experiments[12,13] have been developed to test the membrane mechanical properties of capsules. The first method is dedicated to local stresses applied to the capsule. The principle is to put a probe in contact with the membrane to study: the compression between two plates,[14] the AFM scanning with a sharp tip[15] or a large colloidal particle[12,16] and the micropipette aspiration.[17] The second method is devoted to global stresses applied to the capsule by means of hydrodynamic flows to study the capsule deformation in a spinning drop apparatus,[18] inside a capillary[19] or in a shear flow.[20,21] Several of these techniques are based on theoretical studies,[22] which are also useful to validate numerical studies.[23–26]

In the elastic regime (*i.e.* under small deformations), the capsule behavior under hydrodynamic stresses has been explored theoretically,[22] giving a relationship between the deformation of the capsule and the surfacic shear modulus. The first experiments which confirmed these predictions were conducted in shear flow[27] based on a cylindrical Couette device and in an elongational flow generated with the so-called four roll mill apparatus.[20]

In this paper, we investigated the mechanical behavior of microcapsules that were manufactured by interfacial cross-linking[28,29] of human serum albumin (HSA) with terephthaloyl chloride in a water-in-oil emulsion system. These microcapsules present the advantage of having a biocompatible, biodegradable and stable membrane for medical applications. The preparation process allowed us to vary easily the HSA concentration. The size distribution of the microcapsules in the different batches was also dependent on the preparation process (Fig. 1).

[a]*Aix Marseille Université, CNRS, Centrale Marseille, IRPHE UMR 7342, 13384 Marseille, France. E-mail: deschamps@irphe.univ-mrs.fr; leonetti@irphe.univ-mrs.fr; Fax: +33 413552001; Tel: +33 413552083*

[b]*Aix Marseille Université, CNRS, CINaM UMR 7325, 13288 Marseille, France*

[c]*Faculté de Pharmacie, Université de Reims Champagne-Ardenne, CNRS, ICMR UMR 7312, 51687 Reims, France*

† Electronic supplementary information (ESI) available: Fig. S1 of the load and unload of the AFM probe during one indentation. See DOI: 10.1039/c4sm00349g

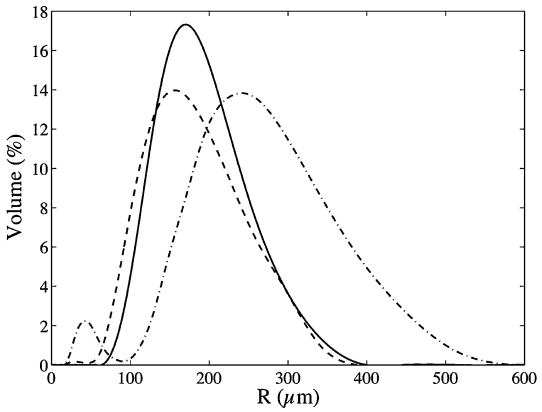

Fig. 1 Size distribution of each batch of capsules: 5% HSA (solid line), 10% (dashed line) and 20% (dash-dotted line).

Two complementary experimental methods were used to determine surfacic and volumic mechanical properties of the membrane in the elastic regime. Studying the deformation of the whole capsule in an elongational (or hyperbolic) flow allowed us to obtain the surfacic shear modulus G_s of the membrane, whereas its volumic Young's modulus E was measured by local and small deformations with an AFM tip. The combination of these surfacic and volumic moduli led to the calculation of the membrane thickness.

2 Materials and methods

2.1 Capsule preparation

Batches of cross-linked HSA microcapsules were prepared using the interfacial cross-linking method,[28,29] with terephthaloyl chloride as the cross-linker. HSA was provided by LFB Biomedicaments, as a 200 mg mL^{-1} solution. This solution has been freeze-dried to vary the HSA concentration for the microencapsulation process. The organic solvents (chloroform and cyclohexane), cross-linking agent (terephtaloyl chloride) and surfactants (sorbitan trioleate and polysorbate) were purchased from SDF, Acros Organics and Sigma, respectively.

Some of the preparation parameters were varied in order to obtain membranes with different cross-linking degrees surrounding liquid droplets of various sizes. Briefly, the HSA solution was prepared at various concentrations (5% m V^{-1}, 10%, 20%) in a pH 8 phosphate buffer. This aqueous solution was emulsified in cyclohexane containing 2% (w/v) sorbitan trioleate at a stirring speed of 625 rpm. A 2.5% (w/v) solution of terephthaloyl chloride in chloroform : cyclohexane (1 : 4 v/v) was then added to the emulsion and the cross-linking reaction was allowed to develop for 30 min. The reaction was stopped by dilution of the reaction medium. The microcapsules were separated from the organic phase by centrifugation and washed successively with cyclohexane, and with water containing 2% (w/v) polysorbate, and finally were transferred into pure water. The granulometric distribution of each batch was determined by laser diffraction using a Malvern Mastersizer 2000 (Fig. 1). In order to be used either in elongational flow or in AFM apparatus, capsules from original batches were diluted to about thousand times and mixed very gently for at least 24 hours in glycerol of 98% of purity (VWR).

2.2 Elongational flow

An elongational flow was generated by using a cross-like channel made of two PMMA plates sealed together. One of the two was first countersunk to create the fluid path and allow image capture (Fig. 2). Two different channels were used with square cross-sections of 1 and 4 mm^2 named thereafter channel 1 and channel 2, respectively. The fluid was injected into the channel through a glass syringe mounted on a home-made syringe pump based on a PI actuator M235-52S. The injection spot was unique. The channel was then split in two symmetrical ways, which were recombined at the stagnation point. Two containers at the ambient pressure were plugged to the two outlets to enable the complete stop of the flow at rest. We paid attention to avoid any deformable pipe and any air bubbles within the whole fluidic system in order to minimize the transient time when the flow was switched on. The visualization was achieved with an inverted microscope Olympus IX-71 with magnification 10 to 16×. A high speed video camera Photron Fastcam SA3 allowed us to acquire up to 5000 frames per second. The image post-processing was performed with Matlab.

Elongational rates were measured by Particle Tracking Velocimetry (PTV). Spherical polystyrene particles of 10 μm diameter (Bangs Laboratories) were seeded in glycerol. The observation area was 1.1 × 1.1 mm^2 seen at 16× in channel 1 and 1.7 × 1.7 mm^2 at 10× in channel 2. The velocity field of the flow was as follows in the plane (x, y) (Fig. 2): $u_x = \dot{\varepsilon}_x$, $u_y = -\dot{\varepsilon}_y$ with $\dot{\varepsilon}$ the elongational rate. We defined a circular area centered at the stagnation point of the flow for which $\dot{\varepsilon}$ was considered homogeneous, *i.e.* with a maximal standard deviation of 5%. For channel 1, the measurement region was of 520 μm diameter. For channel 2, which had its corners cut in the cross-like region, the measurement area was of 1300 μm diameter. $\dot{\varepsilon}$ was averaged over these regions. The deformation of the capsules was analyzed exclusively in these regions. The flow rate was varied from 10 to 500 μL s^{-1} to measure the elongational rate at the middle of the thickness of the channel. We found a linear dependence of the elongational rate on the flow rate (Fig. 3) for both channels.

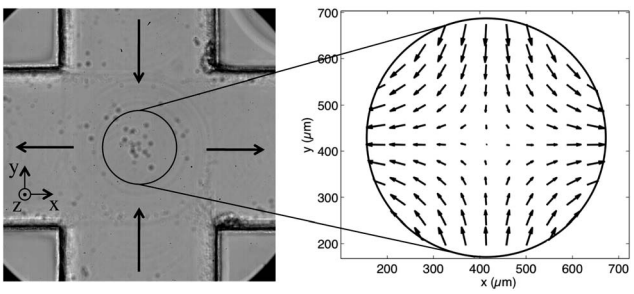

Fig. 2 Left: an image of channel 1. The cross-like channel width is 1 mm. Arrows show the flow direction. The circle defines the region where the elongational rate variation does not exceed 5%. Right: an example of velocity field obtained within the measurement area with PTV.

The dependence of $\dot{\varepsilon}$ on the depth of the channel was determined (z direction). The flow rate was kept constant at 17 μL s^{-1}. $\dot{\varepsilon}$ was measured through the thickness of the channel to determine its variation with the depth z. As expected, the flow had a Poiseuille-like profile (Fig. 4). For the measurement of the shape of capsules in the elongational flow, its z position was measured to determine accurately the elongation rate using the law $\dot{\varepsilon} = f(z)$ determined in Fig. 4. To prevent any effect of the channel walls, only capsules close to the center (*i.e.* distance from the center below ± 200 μm) were studied.

To deduce the stress $\eta\dot{\varepsilon}$, the viscosity η of glycerol was measured with a rheometer ThermoScientific Haake Mars III in a cone–plate geometry (2° cone, 60 mm diameter) in order to get a correction of the viscosity with the temperature. The temperature of the sample was regulated by an integrated Peltier effect system that heated the plate of the cone–plate measurement configuration. The regulation system ensured that the temperature of the lower plate was accurate to within ±0.1 °C. The measurement geometry was enclosed in an envelope that acts as a solvent trap, thus considerably reducing evaporation on the unconfined surface of the sample. It also reduced heat losses and ensured a uniform temperature around the sample. Calibration with a standard oil (Paragon Scientific Ltd) of viscosity similar to that of glycerol showed that the standard error on the viscosity measurement was below ±2.5%. A digital thermometer, that was calibrated with the Peltier system of the rheometer, was inserted very close to the channel to get the temperature with a precision of 0.1 °C. All experiments were carried out at a temperature range of 22 °C ± 0.5 °C.

The deformation of an elastic capsule under flow can be evaluated by the dimensionless ratio of the viscous stress $\eta\dot{\varepsilon}$ on the elastic response G_s/R. This is the capillary number Ca:

$$\mathrm{Ca} = \frac{\eta\dot{\varepsilon}R}{G_s} \tag{1}$$

where R is the radius of the capsule in the resting state (Fig. 5), η is the viscosity of the outer fluid and $\dot{\varepsilon}$ is the rate of deformation due to a shear or elongational flow. Various constitutive laws may describe the linear and non-linear behaviour of a cross-linked polymer membrane such as Neo-Hookean, Skalak or Mooney Rivlin.[30] However, all these models reduce to Hooke's law in the limit of small deformations and thus leading to the same mechanical moduli. The membrane mechanics of a thin 3D isotropic material can be modelled by a surfacic constitutive law without bending resistance and with the following relationship between the relevant mechanical quantities:

$$G_s = \frac{E_s}{2(1+\nu)} \tag{2}$$

$$E_s = Eh \tag{3}$$

where G_s is the surfacic shear elastic modulus, ν is the Poisson ratio, E_s and E are the 2D and 3D Young's moduli and h is the thickness of the membrane. The Poisson ratio ν was assumed to be equal to 1/2 (*i.e.* the membrane is considered as an incompressible material).

The projection in the plane (x, y) of the deformed capsule was assumed to be an ellipse of major and minor semi-axis lengths L and B. In the small deformation regime, the deformation is evaluated by the shape parameter (Fig. 5):

$$D = \frac{L-B}{L+B}$$

Capsules were trapped one by one at the stagnation point of the elongational flow (Fig. 1). This was achieved by regulating

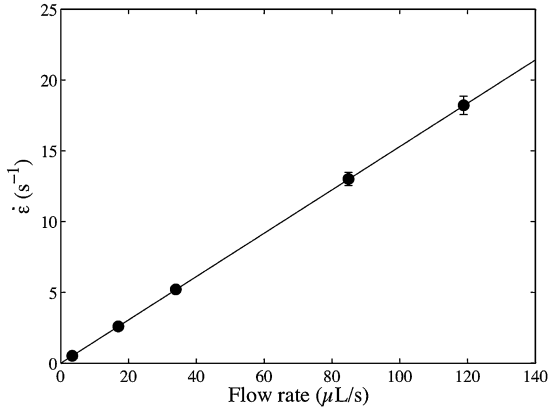

Fig. 3 Elongational rate as a function of the flow rate for channel 2. Only the upper half is plotted.

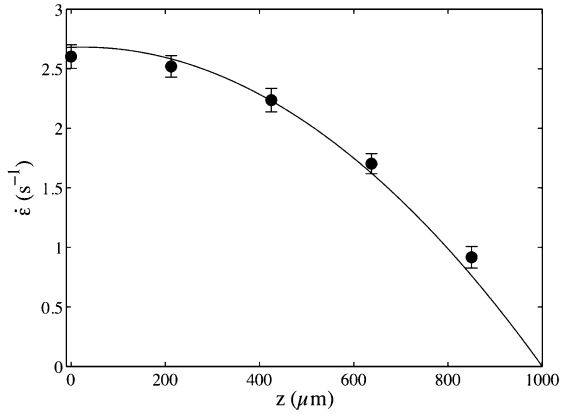

Fig. 4 Elongational rate as a function of the elevation z for channel 2.

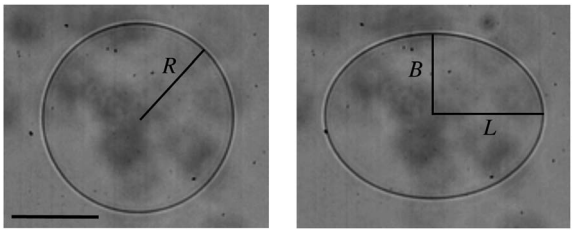

Fig. 5 Image of a capsule of radius R at rest (left). On the right the same capsule deformed by the elongational (or hyperbolic) flow. L and B are the major and minor semi-axis respectively. Notice that the deformation is large (14%) compared to what has been realized in the paper. Scale bar is 100 μm.

the hydrostatic pressure at the outlets and by moving back and forth the piston of the syringe as often as necessary. When the capsule was stabilized, we applied suddenly the flow and measured the deformation D of the capsule as a function of time. D saturated to a stationary value called D_∞ (Fig. 6). The measurement area was large enough for the capsule to reach a stationary deformation before it was carried away by the flow. For each capsule, we repeated several times the same experiment at different elongational rates by bringing the capsule backward to the stagnation point. Finally, it has been shown theoretically that D_∞ varies linearly with the capillary number $D_\infty = 25/6$ Ca.[30] Thus using eqn (1), the determination of G_s is given by:

$$G_s = \frac{25}{6}\frac{\eta R\dot{\varepsilon}}{D_\infty} \quad (4)$$

2.3 AFM

Force measurements were carried out in glycerol using AFM (NTEGRA from NT-MDT). sQube colloidal probes with a silicon dioxide bead and the resonance frequency in the range 6–21 kHz were purchased from NanoAndMore. Probe tip radii were determined after imaging the tip by scanning electron microscopy and a radius of 0.95 μm was found for every tip. Spring constants ranging from 0.03 to 0.13 N m^{-1} were determined using the thermal noise method after obtaining the deflection sensitivity of the cantilever by pressing the AFM tip against a hard reference glass bead of the 70 GPa Young's modulus. Cantilever deflection sensitivity measurements were performed before all sets of measurements. Force measurements were realized at a loading rate of 1600 nm s^{-1} and the indentation depth was maintained below 150 nm for most samples. For each capsule, statistical analysis was realized with a minimum of 200 force measurements obtained from a total area of 15 × 15 μm^2. To extract the Young's modulus, each curve was fitted using the Hertz model (see ESI† for the fitting model) of contact between two spheres according to the following equation:

$$F = \frac{4}{3}\frac{\tilde{R}^{1/2}\delta^{3/2}}{(1-\nu_t^2)/E_t + (1-\nu_c^2)/E_c}$$

with F being the force applied by the tip on the capsule, $E_t = 150$ GPa and E the Young's moduli of the tip and the capsule and $\nu_t = \nu = 0.5$ the Poisson ratios of the tip and the capsule respectively. $\tilde{R} = (1/R + 1/R_t)^{-1}$ with R and R_t being the capsule and tip radii respectively, and δ the indentation. As verified experimentally in this range of indentation, this model assuming an elastic behavior of the capsules is valid.

3 Results and discussion

3.1 Surfacic shear modulus

Fig. 6 shows the typical deformation curves as a function of time for one capsule (20% HSA) and four elongational rates. The stationary deformation D_∞ was defined as the plateau value of the curve $D(t)$ at steady state. In Fig. 7, we report this maximal deformation as a function of the hydrodynamic stress $\eta\dot{\varepsilon}$. As predicted from theory,[22] small deformations increase linearly with the stress. All the capsules were observed within the linear elastic regime, typically $D < 6\%$ in this paper. In fact, all the individual curves D_∞ as a function of the stress were fitted with a linear regression. Typically, the reliability factor values varied from 0.92 to 1. Moreover, some capsules were not perfectly spherical and could be characterized by an initial deformation D_0 in the resting state. Only capsules with $D_0 < 0.2\%$ were analyzed. After the hydrodynamic stress was applied, the capsule recovered its initial shape, *i.e.* its radius R and its initial deformation D_0 did not vary. Thus, experiments were carried out in the elastic regime.

Each capsule was tested for about four to six different values of elongational rates covering a range with at least a factor 2. The surfacic shear modulus G_s for each run was calculated by eqn (4) and then averaged over a full set of runs for each capsule. Fig. 8 shows the variation of G_s with the capsule radius R for 10% HSA. Notice that measurements are independent of the size of the channel.

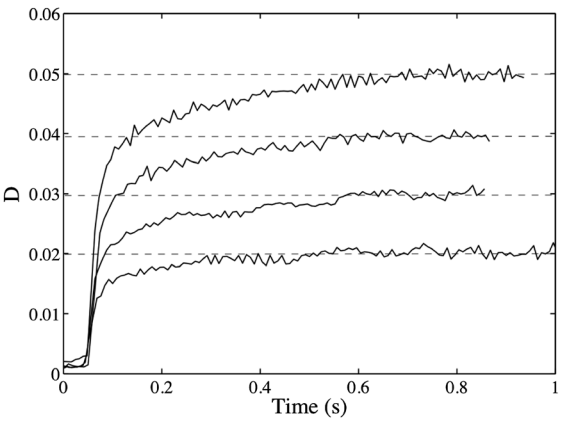

Fig. 6 Deformation parameter D for one capsule (20% HSA) and four elongational rates: 3.53 s^{-1}, 5.30 s^{-1}, 7.13 s^{-1}, and 9.04 s^{-1}. D_∞ was extracted as the plateau of each curve and is emphasized here by the dotted lines.

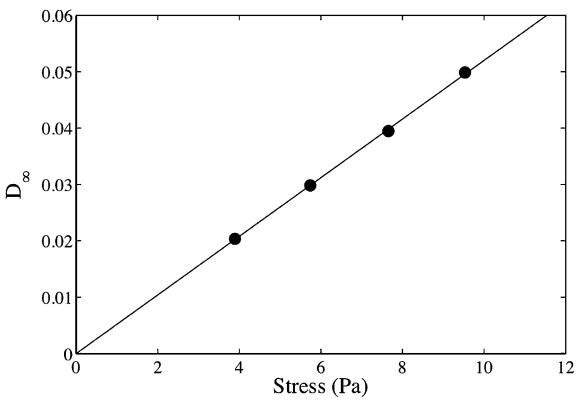

Fig. 7 The deformation D_∞ as a function of the stress for the capsule (20% HSA) shown in Fig. 6. The linear regression depicts the linear elastic regime.

The results of G_s for the three HSA concentrations (5, 10 and 20%) are shown in Fig. 9. As the size of the capsule increases, the surfacic shear modulus strongly non-linearly rises. For 10% HSA, a factor 3.5 in size gives a factor 2000 in G_s. Small capsules (about 70 μm radius) exhibit a G_s of the order of 10^{-2} N m^{-1} whereas a larger one (about 160 μm radius) is characterized by a G_s of about 5 N m^{-1}. Compared to the size distribution of the capsules for each HSA concentration (Fig. 1), the measurements of G_s were limited to capsules whose radius was less than 200 μm. In fact, the experimental area where measurements are valid (see Fig. 2) was too small to observe steady deformations for radii larger than 200 μm. Furthermore capsules with 10 and 20% HSA larger than 170 μm were too rigid to be sufficiently elongated with our experimental set-up. Capsules with 5% HSA smaller than 100 μm were non-spherical at rest, so that no data are reported in the figure. The method consisting in subtracting the initial deformation D_0 to D[18] was not applicable here since the initial deformation is not systematically elliptic.

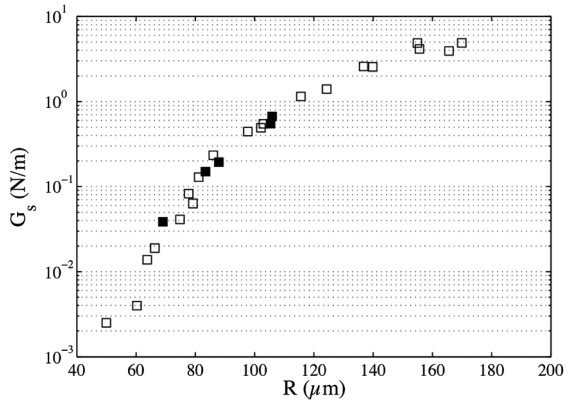

Fig. 8 Surface shear modulus for capsules with 10% HSA as a function of the radius R. Open squares: capsules in channel 1. Filled squares: capsules in channel 2.

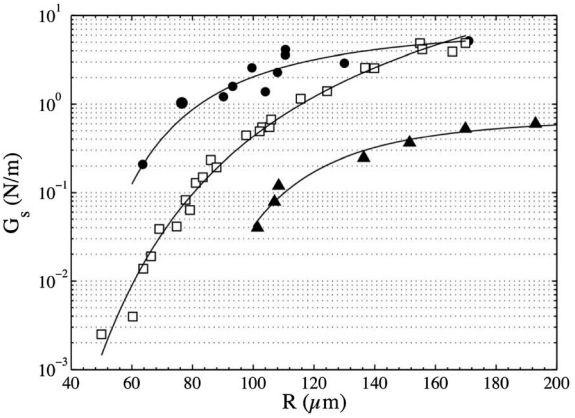

Fig. 9 Surfacic shear modulus as a function of the radius R and the rate of HSA. Lines are the interpolation of data points with the function $\log(G_s) = ax^b + c$. See values of (a, b, c) for each batch below in the text. Circles: 20% HSA capsules. Squares: 10% HSA capsules. Triangles: 5% HSA capsules. The error bar on each point is less than 6%, it means less than the size of the three symbols.

The large range of sizes accessible with the present method and its resolution allowed us to measure G_s in the elastic regime ($D_\infty < 6\%$) and to show its variation with capsule size and HSA concentration. None of the former studies on other kinds of capsules have mentioned the variation of G_s according to the size.[20] It was even avoided for capsules based on the polysiloxane network[18] for which attention was paid to keep the membrane constitution equivalent regardless of the size. Our results show (Fig. 8) that the effect of the size on G_s is less important for large capsules than for small capsules. Thus, measuring G_s with an elongational flow offers both a very small degree of dispersion of the measurements and a method to investigate accurately the dependence of G_s with the process parameters. However, capillary experiments[19] have to be preferred for large and rigid capsules since it is easy for applying higher stresses.

The shear modulus is much dependent on the HSA concentration. In Table 1, G_s values are reported for radii about 107 μm. As the quantity of proteins increases in the emulsification preparation by a factor 4, the resistance of the membrane to shear is multiplied by 30. This behavior is consistent with other observations on capsules prepared with various materials.[18,21,31]

The elongational method is peculiarly accurate to measure the surfacic shear modulus G_s characterized by an error less than 6% for each capsule. It means that the deviations larger than this error result only from the capsule processing. Such a dependence was expected as the processing is complex and involves some chemical reactions, a biphasic system, diffusion of molecules and an hydrodynamic flow, the interfacial polymerization taking place during the solution mixing. As shown in Fig. 9, the deviation increases with the HSA concentration and is larger for the batch 20% and smaller for the batch 10%.

3.2 Volumic Young's modulus

Similar to the surfacic shear elastic modulus G_s, the volumic Young's modulus E of the capsule membrane varies with the size R of the capsules (Fig. 10) whatever be the HSA concentration. Due to the difficulty of these measurements, experimental data do not cover the same range of size for each batch than the previous hydrodynamic study. One limiting step is given by the lubrification phenomenon in the thin glycerol film between the substrate and the capsule governing the time to reach the stationary state. During an indentation of depth δ with a maximum of the order of 100 nm, the zone of deformation extends to the characteristic length $l \approx \sqrt{\delta r}$ where $r = 0.95$ μm is the tip size of the AFM probe: $l \approx 0.3$ μm. This order of magnitude is sufficiently small compared to the capsule size

Table 1 Variation of G_s for radii about 107 μm

Capsules	R (μm)	G_s (N m^{-1})
5% HSA	107.0	0.078 ± 0.0023
10% HSA	105.9	0.669 ± 0.014
20% HSA	108.4	2.29 ± 0.095

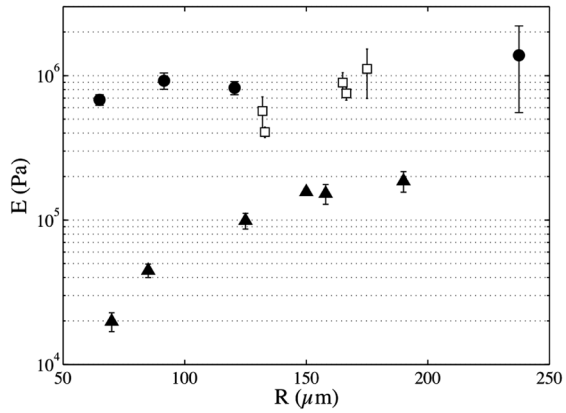

Fig. 10 Young's modulus E of the membrane measured with AFM for the different HSA concentrations. Circles: 20% HSA capsules. Squares: 10% HSA capsules. Triangles: 5% HSA capsules.

and the expected membrane thickness to insure the relevance of the Hertz law (see Materials and methods).

AFM experiments are local while deformations of a capsule in an elongation flow depend on the global shape. Thus the non-sphericity of the capsule does not affect the measurement as it is the case for capsules with 5% HSA smaller than 100 μm in the elongational flow.

The smallest observed capsule leads to a Young's modulus of about 0.02 MPa whereas for the largest one, E is 100 times larger. Considering the HSA concentration, we qualitatively observe the same behavior as for G_s: E increases by one order of magnitude as the HSA rate increases from 5 to 20%. However, this dependence is weaker for batches 10 and 20% HSA. This indicates that the properties of the polymer network saturate with an increase of the HSA concentration. Indeed, batches 10 and 20% HSA give the same E and the same G_s for capsules of 170 μm radius which emphasizes that both E and G_s are correlated. Contrarily, the Young's modulus increases clearly with the capsule radius for 5% HSA. No variation of E with the size of the capsule has been reported elsewhere even for capsules made of other kinds of albumin such as ovalbumin.

3.3 Membrane thickness

In this part, it is shown that the two previous measurements by two complementary experiments allow us to infer the thickness of the capsule membrane. As the data of Young's modulus are sparse, only orders of magnitude can be evaluated.

So far the membrane has been considered as a 2D medium but due to the interfacial cross-linking reaction, the membrane has a finite thickness h. It was assumed in previous studies on capsules made of albumin that the thickness is constant in a batch. Thereafter, the wall is considered to be homogeneous. h is not measurable with the experiment in elongational flow. Usually it is either accessible with fluorescence microscopy if possible[32] or with electronic microscopy[33] after a dehydration step of the capsule, which often affects the dimensions of the membrane as compared to the wet state. Instead of measuring it with classical methods, the previous experiments performed in the linear elastic regime allowed us to calculate it indirectly but in real suspension.

According to eqn (2) and (3), h is given by: $h = 3G_s/E$. In order to obtain same size values for capsules to be associated with both experiments, arbitrary interpolations on data points from the hydrodynamic experiments were determined (Fig. 9) with the following regression: $\log(G_s) = ax^b + c$. The following values (a, b, c) values were obtained: capsules 5% HSA ($-1.13\ 10^8$, -3.799, -0.3372), capsules 10% HSA (-326.6, -0.8217, 6.579), capsules 20% HSA ($-3.30\ 10^4$, -2.194, 2.061). Consequently, the thickness of the membrane was calculated only for the range of capsule sizes that are covered by hydrodynamic experiments.

The thickness increases with the capsule size (Fig. 11), notably in the case of batches 10 and 20% HSA. Moreover, at a fixed radius, the thickness grows with the concentration of HSA. These variations can be qualitatively understood, considering the capsule-processing. One limit case is the cross-linking of all molecules of HSA in the drop at the interface. A simple mass balance shows that the thickness should increase linearly with the capsule radius R and with the bulk HSA concentration C^{3D}_{HSA} in the case of a homogeneous membrane: $h = 3G_s/E = (R/3)(C^{3D}_{HSA}/C^{2D}_{HSA})$ where C^{2D}_{HSA} is the concentration of HSA in the membrane. This relationship is qualitatively satisfied by our results, which combine deformation in an elongation flow and AFM studies. However, the chemical association at the interface is more complex. After the first layer of HSA covers the interface between oil and water, new HSA needs to cross over the layer to reach the terephthaloyl chloride to have the continuation of the cross-linking reaction. As the layer thickens, the transfer becomes limited by its permeability to HSA. Thus C^{2D}_{HSA} is more an effective quantity, which takes into account a complex chemical process at the interface associated with a thickening which could result in a non-homogeneous membrane. A deeper understanding needs a better knowledge of kinetic constants, Marangoni-like and flow effects during interfacial polymerization.

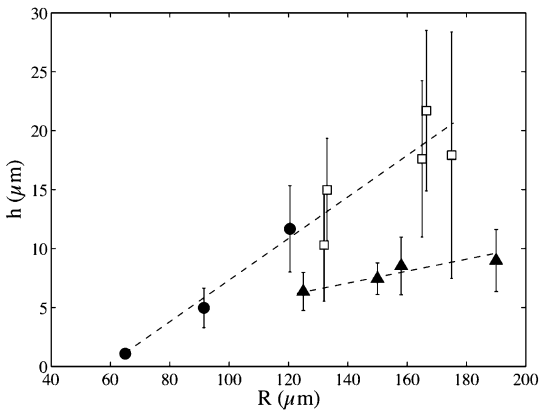

Fig. 11 The calculated thickness h of the capsule membrane as a function of the size R. Circles: 20% HSA capsules. Squares: 10% HSA capsules. Triangles: 5% HSA capsules. The dashed lines are a guide to the eye.

For the batch 20% HSA the wall accounts from 1.6% of the radius for a capsule of radius 64 μm to 9% for 120 μm. The same increase is observed for 10% HSA capsules, which reaches about 11% for a capsule about 170 μm. A different behavior is pointed out for 5% HSA capsules, which have a constant ratio of about 5%. This could question the validity of the assumption of an infinitely thin membrane in theoretical and numerical studies.

4 Conclusions

In this paper the capsule processing based on the interfacial cross-linking method is studied by investigating the mechanical properties of the capsule membranes produced at a given emulsification rate. For each batch characterized by one concentration of HSA, the distribution of sizes has one or two peaks with a typical range from 100 to 300 μm for 5% HSA for example (Fig. 1). In each batch, the mechanical properties of capsules have been measured following two parameters: the initial concentration of human serum albumin in the aqueous solution and the radius of the capsule, which is a consequence of the processing. Both surfacic and volumic Young's moduli have been extracted from small deformations (linear elastic regime) observed in two complementary experiments. The surfacic shear modulus G_s, which is linear to the surfacic Young's modulus, is determined by the extensions of individual capsules plunged in an elongational flow with different magnitudes. The volumic Young's modulus E is deduced from the AFM force–indentation curves provided by local deformations of the membrane in the linear elastic regime. Note that the method based on an elongational flow has only been used one time previously and on capsules of several millimeters of radius using the famous four roll mills technique. Here, we extend the elongation method to capsules of typical radius of 100 μm with a microfluidic-like chip.

As expected G_s and E depend largely on the protein concentration of the primary droplet. Surprisingly we observe an enhanced behavior of the two elastic moduli with the size: typically 3 orders of magnitude for G_s for only a factor 3 in the capsule size (10% HSA). This unexpected strong variation is partly explained by the large variation of the volumic Young's modulus characterizing the polymer network of the membrane measured by AFM. However this is not enough to explain fully the variation of G_s. The other salient contribution is due to the variation of the membrane thickness with concentration and size. The thickness is deduced from the combination of the values of the surfacic shear elastic modulus and the volumic Young's modulus measured independently. For large sizes of capsules, G_s, E and h saturate above 10% HSA rates. A material balance applied between membrane HSA and volumic available HSA before polymerization explains the qualitative variation with the size and HSA concentration but is not quantitative to fully capture the understanding of the processing.

Nevertheless the relationship between size and mechanical properties gave highly sought information in terms of applications. In the field of chimioembolization the size and the resistance of the capsule have to be adjusted to the vessel to fill up. Moreover the data obtained should be used to optimize the release kinetics of the encapsulated substances as in the field of cosmetic for which capsules, according to their size, should be used either to break under finger pressure or to deliver slowly their inner material through the intact membrane. As the capsule size and mechanical properties are related, one way to reach the desired value of the capsule rigidity is to adjust its size. Even if initial size distributions are pretty wide due to the preparation process, various methods[34] have been developed to sort particles in much narrower size distributions.

Experiments in elongational flow were conducted in the regime of small deformations in order to determine linear mechanical properties of microcapsules. Investigations in the large deformation regime should give valuable information enabling the determination of the constitutive law of the HSA membrane and its breakdown properties.

Acknowledgements

This work has benefited from the financial support of CNES. This work has also been carried out in the framework of the ANR CAPSHYDR (11-BS09-013-02), of the ANR polytransflow (13-BS09-0015-01), of the Labex MEC (ANR-10-LABX-0092) and of the A*MIDEX project (ANR-11-IDEX-0001-02), funded by the Investissements d'Avenir French Government program managed by the French National Research Agency (ANR).

References

1 A. Madene, M. Jacquot, J. Scher and S. Desobry, *Int. J. Food Sci. Technol.*, 2006, **41**, 1–21.
2 C. Onwulata, *Annu. Rev. Food Sci. Technol.*, 2012, **3**, 183–202.
3 R. Fernandes and D. H. Gracias, *Adv. Drug Delivery Rev.*, 2012, **64**, 1579–1589.
4 D. Demirgöz, T. O. Pangburn, K. P. Davis, S. Lee, F. S. Bates and E. Kokkoli, *Soft Matter*, 2009, **5**, 2011–2019.
5 S. Banquet, E. Gomez, L. Nicol, F. Edwards-Lévy, J.-P. Henry, R. Cao, D. Schapman, B. Dautreaux, F. Lallemand, F. Bauer, *et al.*, *Circulation*, 2011, **124**, 1059–1069.
6 R. K. Shah, J.-W. Kim, J. J. Agresti, D. A. Weitz and L.-Y. Chu, *Soft Matter*, 2008, **4**, 2303–2309.
7 A. G. Skirtach, B. G. De Geest, A. Mamedov, A. A. Antipov, N. A. Kotov and G. B. Sukhorukov, *J. Mater. Chem.*, 2007, **17**, 1050–1054.
8 S.-H. Hu, C.-H. Tsai, C.-F. Liao, D.-M. Liu and S.-Y. Chen, *Langmuir*, 2008, **24**, 11811–11818.
9 Y.-C. Tan, K. Hettiarachchi, M. Siu, Y.-R. Pan and A. P. Lee, *J. Am. Chem. Soc.*, 2006, **128**, 5656–5658.
10 U. Seifert, *Adv. Phys.*, 1997, **46**, 13–137.
11 D. E. Discher and F. Ahmed, *Annu. Rev. Biomed. Eng.*, 2006, **8**, 323–341.
12 A. Fery and R. Weinkamer, *Polymer*, 2007, **48**, 7221–7235.
13 Z. Zhang, J. Stenson and C. Thomas, *Adv. Chem. Eng.*, 2009, **37**, 29–85.
14 F. Risso and M. Carin, *Phys. Rev. E: Stat., Nonlinear, Soft Matter Phys.*, 2004, **69**, 061601.
15 M. Radmacher, *Methods Cell Biol.*, 2002, **68**, 67–90.

16 F. Dubreuil, N. Elsner and A. Fery, *Eur. Phys. J. E: Soft Matter Biol. Phys.*, 2003, **12**, 215–221.
17 R. M. Hochmuth, *J. Biomech.*, 2000, **33**, 15–22.
18 I. Koleva and H. Rehage, *Soft Matter*, 2012, **8**, 7672–7682.
19 Y. Lefebvre, E. Leclerc, D. Barthès-Biesel, J. Walter and F. Edwards-Lévy, *Phys. Fluids*, 2008, **20**, 123102.
20 K. Chang and W. Olbricht, *J. Fluid Mech.*, 1993, **250**, 609–633.
21 I. Koleva and H. Rehage, *Soft Matter*, 2012, **8**, 3681–3693.
22 D. Barthes-Biesel and J. M. Rallison, *J. Fluid Mech.*, 1981, **113**, 251–267.
23 S. Ramanujan and C. Pozrikidis, *J. Fluid Mech.*, 1998, **361**, 117–143.
24 C. Pozrikidis, *J. Comput. Phys.*, 2001, **169**, 250–301.
25 E. Lac and D. Barthès-Biesel, *Phys. Fluids*, 2005, **17**, 072105.
26 W. D. Dodson III and P. Dimitrakopoulos, *J. Fluid Mech.*, 2009, **641**, 263–296.
27 K. Chang and W. Olbricht, *J. Fluid Mech.*, 1993, **250**, 587–608.
28 M.-C. Andry, F. Edwards-Lévy and M.-C. Lévy, *Int. J. Appl. Pharm.*, 1996, **128**, 197–202.
29 T. Chu, A.-V. Salsac, E. Leclerc, D. Barthès-Biesel, H. Wurtz and F. Edwards-Lévy, *J. Colloid Interface Sci.*, 2011, **355**, 81–88.
30 E. Lac, D. Barthes-Biesel, N. Pelekasis and J. Tsamopoulos, *J. Fluid Mech.*, 2004, **516**, 303–334.
31 S. Leick, A. Kemper and H. Rehage, *Soft Matter*, 2011, **7**, 6684–6694.
32 H. G. Bagaria, S. B. Kadali and M. S. Wong, *Chem. Mater.*, 2010, **23**, 301–308.
33 E. Brown, M. Kessler, N. Sottos and S. White, *J. Microencapsulation*, 2003, **20**, 719–730.
34 A. Srivastav, T. Podgorski and G. Coupier, *Microfluid. Nanofluid.*, 2012, **13**, 697–701.